Magnetic Resonance in Medicine

T$_2$-oximetry–based cerebral venous oxygenation mapping using Fourier-transform–based velocity-selective pulse trains

Wenbo Li[1,2] | **Feng Xu**[1,2] | **Dan Zhu**[1,2] | **Peter C. M. van Zijl**[1,2] | **Qin Qin**[1,2]

[1]The Russell H. Morgan Department of Radiology and Radiological Science, Division of MR Research, Johns Hopkins University School of Medicine, Baltimore, Maryland, USA

[2]F.M. Kirby Research Center for Functional Brain Imaging, Kennedy Krieger Institute, Baltimore, Maryland, USA

Correspondence
Qin Qin, Department of Radiology, Johns Hopkins University School of Medicine, F.M. Kirby Research Center for Functional Brain Imaging, Kennedy Krieger Institute, 707 N. Broadway, Baltimore, MD, 21205, USA
Email: qqin1@jhu.edu

Funding information
Supported by funding from the National Institutes of Health (NIH), grants P41 EB031771, P50 HD103538, S10 OD021648 (**P.C.M.VZ**); NIH grants K25 HL145129 (**W.L.**); and NIH grants R01 HL138182, R01 HL144751 (**Q.Q.**).

Purpose: To develop a T$_2$-oximetry method for quantitative mapping of cerebral venous oxygenation fraction (Y$_v$) using Fourier-transform–based velocity-selective (FT-VS) pulse trains.

Methods: The venous isolation preparation was achieved by using an FT-VS inversion plus a nonselective inversion (NSI) pulse to null the arterial blood signal while minimally affected capillary blood flows out into the venular vasculature during the outflow time (TO), and then applying an Fourier transform based velocity selective saturation (FT-VSS) pulse to suppress the tissue signal. A multi-echo readout was employed to obtain venous T$_2$ (T$_{2,v}$) efficiently with the last echo used to detect the residual CSF signal and correct its contamination in the fitting. Here we compared the performance of this FT-VS–based venous isolation preparations with a traditional velocity-selective saturation (VSS)–based approach (quantitative imaging of extraction of oxygen and tissue consumption [QUIXOTIC]) with different cutoff velocities for Y$_v$ mapping on 6 healthy volunteers at 3 Tesla.

Results: The FT-VS–based methods yielded higher venous blood signal and temporal SNR with less CSF contamination than the velocity-selective saturation–based results. The averaged Y$_v$ values across the whole slice measured in different experiments were close to the global Y$_v$ measured from the individual internal jugular vein.

Conclusion: The feasibility of the FT-VS–based Y$_v$ estimation was demonstrated on healthy volunteers. The obtained high venous signal as well as the mitigation of CSF contamination led to a good agreement between the T$_{2,v}$ and Y$_v$ measured in the proposed method with the values in the literature.

KEYWORDS
arterial nulling, cerebral venous oxygenation, mitigate CSF contamination, velocity-selective pulse train, venous cerebral blood

1 | INTRODUCTION

Regional mapping of cerebral venous oxygenation fraction (Y_v) is required for hemodynamic assessment of brain oxygen consumption. MRI techniques for voxel-wise Y_v mapping are mainly based on the fact that hemoglobin changes its magnetic property from diamagnetic to paramagnetic when dissociated with oxygen, such as asymmetric spin echo,[1,2] respiratory-calibrated fMRI,[3–7] quantitative BOLD (qBOLD),[3,6,8–11] quantitative susceptibility mapping (QSM) with microvascular[12–14] or microvascular models,[15–17] the combination of qBOLD and QSM,[18–20] and quantitative venous T_2 ($T_{2,v}$) methods.[13–16] Compared to the other methods that rely on sophisticated signal models of the extravascular tissue and the deoxygenated venous blood, T_2-oximetry methods such as QUIXOTIC[21,22] and VSEAN[23,24] were developed with direct isolation of the local venous blood signal and the measurement of $T_{2,v}$.

In contrast to the more widely used T_2-oximetry methods that obtain global Y_{va} from large cerebral veins,[25–27] regional Y_v mapping techniques are inherently SNR-limited due to the limited amount of venous blood in each voxel, with a volume fraction of only about half of the total cerebral blood volume (CBV) and 2%–3% of the cerebral parenchymal volume.[28–30]

The QUIXOTIC method first utilized a "sinc" modulated velocity-selective saturation (VSS) pulse train followed by a NSI pulse to null the arterial blood signal, which also attenuated the venous signal substantially during the outflow. The second VSS module was applied right before the acquisition with interleaved label and control pulse trains to subtract out the signal from the static tissue, which can introduce considerable error from the much larger tissue background signal. To increase SNR, the VSEAN method applied a slab-selective inversion under the imaging plane to null the incoming arterial blood while retaining the venous blood signal in the imaging plane.[23] However, this approach is sensitive to the arterial transit time, which is not ideal for a large spatial coverage or patients with ischemic regions. For better suppression of static tissue signal, VSEAN used a "sine" modulated VS module twice to specifically excite the slow-moving spins without control-label acquisitions and subtraction.[23] Although this unique technique would alleviate the background noise from static tissues, the double VS module application results in additional signal attenuation. Furthermore, VSEAN requires a phase-based signal projection procedure for flow signal separation, which is less straightforward than subtraction-based methods.

Based on the laminar flow distribution within the vessels, the "sinc" modulated VSS pulse trains saturate the magnetization of spins flowing above a cutoff velocity (V_{cut}) while preserving the magnetization of spins flowing below V_{cut}. VSS-based label and control modules have been employed for MR angiography (MRA)[31–33] as well as measuring cerebral blood flow,[34,35] total CBV,[36] and venous CBV (vCBV).[37] Conversely, the emerging Fourier-transform–based velocity-selective (FT-VS) pulse trains preserve magnetization of spins flowing above a V_{cut} and saturate (FT-VSS) or invert FT-velocity selective inversion (FT-VSI) the magnetization of spins flowing below V_{cut}, and have been applied to MRA[38–44] as well as measuring cerebral blood flow.[45–51] When quantifying total CBV,[52] FT-VSS–based label and control modules have been shown to achieve more effective suppression of the tissue background noise than VSS preparations. Recently, a technique for estimating vCBV[53] was proposed by using FT-VSI and NSI pulses for arterial-nulling and FT-VSS–based label and control modules for tissue suppression. Compared to the VSS-based arterial-nulling as used in QUIXOTIC, FT-VSI can potentially reduce the attenuation of the venous signal during the outflow and achieve higher SNR.

Obtaining images at multiple echo times within each TR has been demonstrated to be feasible for a more efficient $T_{2,v}$ fitting.[22] A further consideration for cerebral Y_v mapping is to mitigate CSF contamination, which arises from either improper labeling due to the pulsatile effect or unmatched diffusion weightings between VS label and control modules. Because the T_2 value of the CSF ($T_{2,CSF}$) is much longer than $T_{2,v}$, images acquired at a long TE can be employed to account for the CSF partial volume effects as proposed previously.[53,54]

In this work, we propose an FT-VS–based cerebral Y_v mapping method by combining the FT-VS–based preparations[53] to isolate the venous signal with high SNR and a multi-echo acquisition scheme to measure $T_{2,v}$[22] and correct for CSF contamination.[53,54] The $T_{2,v}$ and Y_v quantifications were compared between the FT-VS–based and the existing VSS-based (QUIXOTIC) Y_v mapping preparations among healthy volunteers at 3 T.
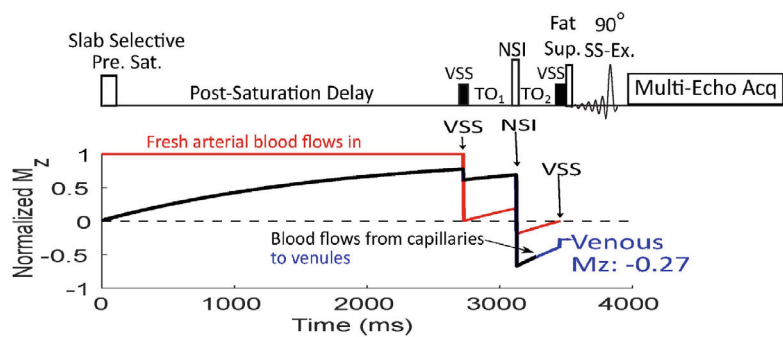
2 | METHODS

2.1 | Pulse sequence

The sequence diagram for FT-VS–based Y_v mapping is shown in Figure 1A. It has the same preparation modules and timing as the sequence for vCBV mapping.[53] A slab-selective presaturation pulse train[55] is used at the start for resetting any magnetization from the previous history, followed by a postsaturation delay of 2500 ms. A spatially nonselective arterial-nulling module, which consists of an FT-VSI pulse train plus an NSI pulse, is followed by an outflow time of 1050 ms based on the arterial T_1 at
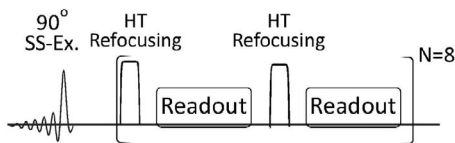
(A) FT-VS:
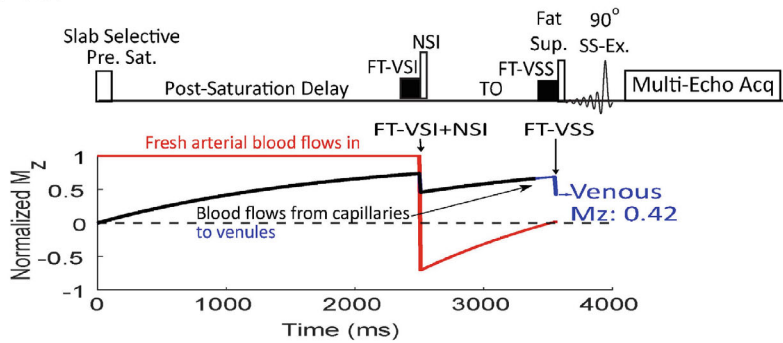
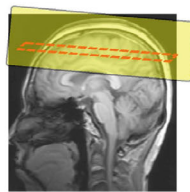## (B) VSS (QUIXOTIC):

(C) Multi-Echo Acq:

(D)

FIGURE 1 Diagrams of the (A) FT-VSS and (B) VSS–based (QUIXOTIC) venous oxygenation (Y_v) mapping methods, including a slab-selective presaturation with a postsaturation delay of ((A) 2500 ms; (B) 2800 ms); an arterial-nulling module ((A) FT-VSI + NSI with outflow time TO = 1050 ms; (B), VSS-TO_1-NSI-TO_2, TO_1/TO_2 = 400/325 ms); label/control pulse trains ((A) FT-VSS; (B) VSS) for tissue suppression, fat-suppression; and (C) a multi-echo readout with 8 pairs of HT refocusing pulses (total of 16 echoes, echo spacing = 15 ms). Simulated magnetization evolution of the arterial (red), capillary (black), and venous (blue) blood during the preparation for both methods are displayed with the T_2-induced signal drop at the FT-VSI/FT-VSS (T_{VS} = 96 ms, V_{cut} = 0.5 cm/s) and VSS (T_{VS} = 25 ms, V_{cut} = 1.0 cm/s) pulse trains included. (D) Location of the imaging FOV (dashed red box) and the presaturation (yellow-shaded rectangular area). FT-VSI, Fourier-transform–based velocity-selective inversion; FT-VSS, Fourier-transform–based velocity-selective saturation; HT, hyperbolic tangent; IJV, internal jugular vein; NSI, nonselective inversion; QUIXOTIC, quantitative imaging of extraction of oxygen and tissue consumption; TO, outflow time; tSNR, temporal SNR; V_{cut} cutoff velocity; VSS, velocity-selective saturation; Y_v, venous oxygenation fraction.

3 Tesla (T) of 1.89 s for a hematocrit (Hct) of 0.42[56,57] and an FT-VSI + NSI inversion efficiency of 0.86.[53] Interleaved scans with FT-VSS label and control pulse trains applied at the end of TO and before imaging are acquired to effectively subtract out the signal of static tissue. Two sets of FT-VS pulse train parameters were compared. One set of the FT-VSS and FT-VSI pulse train blocks have a duration of T_{VS} = 96 ms with triangular gradient lobes (G_{VS} = 29 mT/m; length: 1.2 ms; ramp time: 0.6 ms; foot–head direction), which yielded a V_{cut} = 0.5 cm/s when defined as the half-width–half-maximum point of the main lobe of the velocity response of the FT-VS pulse train. Note that, although the same RF and gradient configurations are used, the previous description of V_{cut} = 0.7 cm/s[53] was defined based on the gradient first moment. The definition of V_{cut} for FT-VS pulse trains adopted in this study allowed closer matching of the labeling with the VSS pulse trains when assuming a laminar flow distribution.[50] The other set of FT-VS pulse trains was applied with a duration of

88 ms with triangular gradient lobes (17 mT/m; length: 0.8 ms; ramp time: 0.4 ms), yielding a V_{cut} = 1.4 cm/s for comparison.

The sequence diagram for VSS–based Y_v mapping is shown in Figure 1B, which has the same preparation modules and timing as the QUIXOTIC studies.[21,22] The VSS pulse trains had a duration of T_{VS} = 25 ms with trapezoid gradient lobes (G_{VS} = 16 mT/m; length: 2.0 ms; ramp time: 0.5 ms) yielding a V_{cut} = 1.0 cm/s when defined as the first zero-crossing of the velocity response under the assumption of laminar flow. Note that this V_{cut} is with regard to the mean blood velocity in the vessels, whereas the previous description of V_{cut} = 2.0 cm/s[21,22] referred to the maximal blood velocity, which is twice the mean velocity.

The simulated magnetization evolutions of the blood spins flowing into the arterioles and venules are illustrated under each sequence diagram. Unlike previous studies,[21,23] the T_2 attenuation effects of both the capillary

and venous blood during the first and second VS pulse trains were taken into account in the present simulation as done for vCBV mapping[53]: assuming Hct of 0.42; Y_v of 0.6 for venous blood; and a modeled capillary oxygen distribution, $T_{2,v}$ = 71 ms, $T_{2,c}$ = 118 ms, for FT-VS and VSS pulse trains with 6 ms and 12.5 ms interecho spacing, respectively. The corresponding T_2 attenuation effects were calculated as −0.62 (0.62 after NSI) for capillary blood and 0.61 for venous blood during the FT-VSI and FT-VSS[53] (Figure 1A), and as 0.79 for capillary blood and 0.70 for venous blood during the first and second VSS pulse trains (Figure 1B), respectively. Hence the estimated magnetization of venous blood after the second VS pulse trains for FT-VS and VSS-based preparations were 0.42 and −0.27, respectively.

A multi-echo acquisition was employed to obtain $T_{2,v}$ efficiently.[22] The last echo (TE = 240 ms) was used to detect the residual CSF signal, which was then used to correct its contamination of the T_2 fitting for venous blood.

2.2 | Experiments

Experiments were conducted on a 3 T scanner (Ingenia, Philips Healthcare, Best, The Netherlands) using the body coil for RF transmission (maximum amplitude 13.5 μT) and a 32-channel head coil for signal reception. The maximum strength and slew rate of the gradient coils were 45 mT/m and 200 mT/m/ms, respectively. The protocol was approved by the institutional review board of Johns Hopkins University School of Medicine, Baltimore, MD. Six healthy volunteers (2 females, 4 males, 34 ± 7 years old) participated in this study, and all provided written informed consent. The FT-VS–based Y_v mapping sequence with V_{cut} of 0.5 cm/s and the VSS-based one with V_{cut} of 1.0 cm/s were applied for each subject. The FT-VS–based sequence using V_{cut} of 1.4 cm/s was applied to 4 of them.

For both the FT-VS- and VSS-based Y_v mapping methods, a total of 16 echoes were acquired with an echo spacing of 15 ms in each TR, and a 2D single-shot EPI was performed as the readout in each echo: a single slice of 10 mm thickness, FOV = 252 × 252 mm² with the acquisition matrix of 32 × 32 and resolution = 7.9 × 7.9 mm², EPI factor = 13, SENSE factor = 2.5. Hyperbolic tangent pulses (4.0 ms, frequency sweep of 11 500 Hz) were used as refocusing pulses with a M.H. Levitt (MLEV)-16 phase-cycling pattern[58] through the 16 echoes. To further alleviate the spurious signal from the imperfect refocusing, excitation pulses of the successive dynamic scans were phase-cycled with 0 and π alternatively.[59] TR was 4.5 s, and 32 dynamic scans were obtained with a total scan time of 5.2 min.

To obtain voxel-wise $T_{2,CSF}$ maps for correcting CSF partial volume for each subject (detailed in Data Analysis

below), a sequence modified from a previous work[60] (Supporting Information Figure S1) was conducted, in which a 600 ms T_2prep module was applied before the multi-echo acquisition to suppress all other signals except CSF. A total of 32 echoes with echo spacing of 15 ms were acquired with the same acquisition parameters as the readout used in $T_{2,v}$ measurements (TR = 10 s; 1.1 min).

With the same FOV and resolution, 2 double inversion recovery (DIR)[61] images were collected to visualize gray matter (TI_1 = 3.58 s; TI_2 = 0.48 s) and white matter (TI_1 = 4.05 s, TI_2 = 0.77 s), respectively (TR = 10 s; 0.9 min). The blood T_1 and T_2 were measured at the internal jugular vein[62,63] to quantify individual Hct and global Y_v[56,64] with about 1.0 min for each scan.

2.3 | Data analysis

MatLab (MatLab R2018b, MathWorks, Natick, MA) was used for data processing. Only even echoes were fitted with a mono-exponential decay model as a function of TEs for both $T_{2,v}$ and $T_{2,CSF}$ values. The $T_{2,CSF}$ maps were first derived from the multi-echo CSF images:

$$S_{CSF} = S_{0,CSF} \times e^{-TE/T_{2,CSF}}. \tag{1}$$

For $T_{2,v}$ quantification, both the $T_{2,CSF}$ map and the difference image between label and control scans of the last echo ($SI_{diff,16}$) were used to estimate the intensity of remaining CSF in the difference image of the nth echo ($SI_{diff,n,CSF}$, n = 1,2, … 15)[54]:

$$SI_{diff,n,CSF} = e^{\frac{(16-n)\cdot\Delta TE}{T_{2,CSF}}} \times SI_{diff,16}, \tag{2}$$

where ΔTE = 15 ms. Hence the CSF-corrected difference image of the nth echo ($SI_{diff,n,CSF-corrected}$) is obtained by subtracting out the CSF contamination ($SI_{diff,n,CSF}$):

$$SI_{diff,n,CSF-corrected} = SI_{diff,n} - SI_{diff,n,CSF}. \tag{3}$$

The corrected images of all 8 even echoes were then smoothed with a 10 mm FWHM Gaussian kernel,[21] then fitted voxel-by-voxel using nonlinear least square algorithm to obtain the $T_{2,v}$ map:

$$S_v = S_0 \times e^{-TE/T_{2,v}}, \tag{4}$$

where S_v is the obtained signal intensity of venous blood at each voxel and S_0 is the fitted amplitude before T_2 decay. Note that a coefficient 0.935 was multiplied to the fitted $T_{2,v}$ values to correct the overestimation induced by the 4 ms pulse length of hyperbolic tangent refocusing pulse
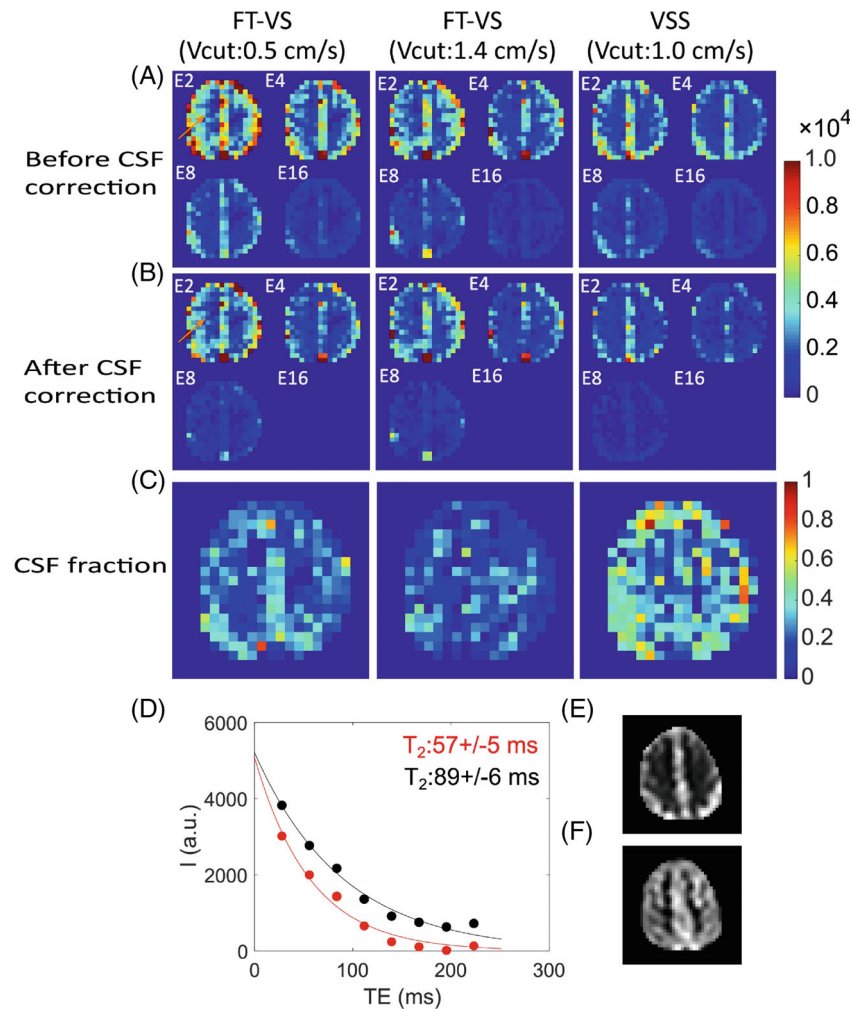
FIGURE 2 Difference images of the second, fourth, eighth, sixteenth echoes (A) before and (B) after CSF correction of a representative subject for the FT-VS–based methods with $V_{cut} = 0.5$ cm/s and 1.4 cm/s; and the VSS-based method with $V_{cut} = 1.0$ cm/s. (C) CSF fraction in the original difference images at the second echo. (D) T_2 fitting of 1 representative voxel (red arrow at the second echo) before (black) and after (red) CSF correction; separately acquired (E) CSF-weighted and (F) DIR-based GM-weighted images. DIR, double inversion recovery; GM, gray matter.

during the 15 ms refocusing interval (Supporting Information Figure S2). The standard errors of the fitted $T_{2,v}$ were reported.

The obtained $T_{2,v}$ map was converted to the Y_v map using the previously developed T_2-Y calibration model[64] with the Hct value estimated from the blood T_1 measured at internal jugular vein (IJV).[56,65] Global Y_v was obtained from the blood T_2 measured at internal jugular vein with the same calibration model. The temporal SNR (tSNR) of the second echo through all the dynamics was also computed for each voxel. The DIR images for gray matter (GM) and white matter (WM) were used to build a mask to calculate averaged Y_v in GM and WM, respectively.

3 | RESULTS

One subject's control and label difference images at 4 different echoes ($SI_{diff,n}$, n = 2, 4, 8, 16) in FT-VS and VSS-based scans are shown in Figure 2A. The corresponding difference images after removing the CSF signal ($SI_{diff,n,CSF-corrected}$) are shown in Figure 2B. The

fraction of remaining CSF in the original difference images at the second echo ($SI_{diff,n,CSF}$ / $SI_{diff,n}$) is displayed in Figure 2C for the 3 sequences. Figure 2D shows that the fitted $T_{2,v}$ with CSF correction (shown in red) reduces the overestimation bias (shown in black). Both FT-VS–based sequences contained less CSF contamination than the VSS-based one (Figure 2C) (Supporting Information Table S1).

Figure 3 arrays another subject's signal intensity and tSNR of the CSF-corrected difference images at the second echo acquired by the 3 sequences, and the maps of quantified $T_{2,v}$ along with the fitting errors ($T_{2,v,error}$). Unlike the difference images (Figure 2B), which have a similar contrast as DIR GM, the fitted $T_{2,v}$ maps and the corresponding Y_v maps show more uniform intensities between GM and WM (Figure 4), as expected for brain OEF. For each sequence, the higher tSNR yielded lower $T_{2,v,error}$ in GM than WM. The tSNR improvement of FT-VS over VSS methods is more notable in GM. Figure 4 shows the DIR GM images, the maps of fitted $T_{2,v}$ and converted Y_v for all 6 subjects, created by applying FT-VS–based protocol using V_{cut} of 0.5 cm/s.
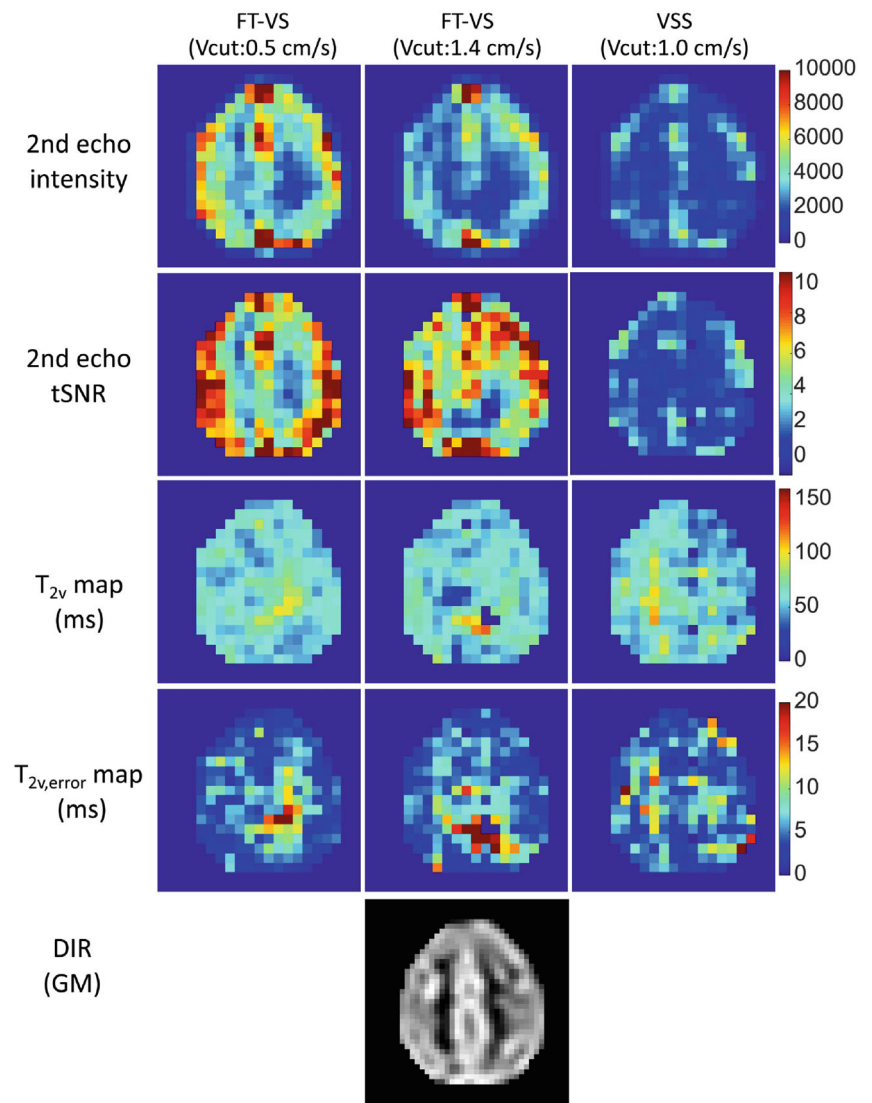
FIGURE 3 Signal intensity and tSNR of the difference images at the second echo after CSF correction of another subject by the FT-VS–based methods with $V_{cut} = 0.5$ cm/s, 1.4 cm/s; VSS-based method with $V_{cut} = 1.0$ cm/s; and corresponding maps of fitted $T_{2,v}$ and fitting errors. DIR-based GM-weighted image is shown as the anatomical reference
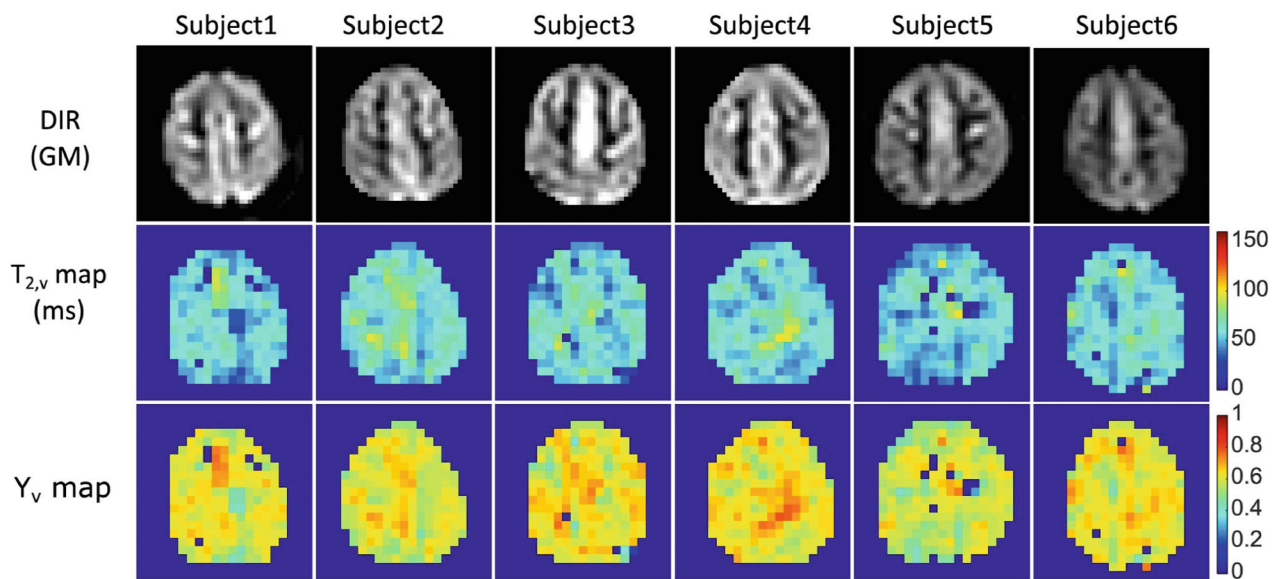

FIGURE 4 DIR-based GM-weighted images, fitted T_{2v} based on the FT-VS–based method with $V_{cut} = 0.5$ cm/s, and converted Y_v maps for all 6 subjects

Table 1 compares the normalized signal intensity and tSNR of the CSF-corrected difference images at the second echo averaged across the slice for each subject, their $T_{2,v}$ with $T_{2,v,error}$, and converted Y_v values with comparison to the global Y_v measured at internal jugular vein. The averaged signal intensities of the difference images by the FT-VS protocol using V_{cut} = 1.4 cm/s and the VSS protocol using V_{cut} = 1.0 cm/s were 31% and 58% lower than those measured by the FT-VS protocol using V_{cut} = 0.5 cm/s (1.00 vs. 0.69 and 0.42). The tSNR in FT-VS experiments was more than twice that in the VSS experiment (5.9 ± 0.9 and 4.8 ± 1.2 vs. 2.3 ± 0.7), which led to 17% and 11% lower $T_{2,v,error}$ comparing FT-VS with VSS experiments (5.3 ± 0.5 and 5.7 ± 0.5 vs. 6.4 ± 0.8). Meanwhile, the whole-slice averaged Y_v values measured in the 2 FT-VS–based (V_{cut} = 0.5 cm/s and 1.4 cm/s) and 1 VSS-based (V_{cut} = 1.0 cm/s) experiments were close to the global Y_v values, as 0.61 ± 0.02, 0.60 ± 0.03, 0.58 ± 0.02, and 0.60 ± 0.03, respectively.

4 | DISCUSSION

In this work, an improved technique is introduced for quantifying regional Y_v by embedding an FT-VS–based preparation module to suppress the static tissue and arterial blood signal and a multi-echo acquisition scheme for T_2 measurement and CSF correction. Compared to the VSS-based preparation (QUIXOTIC), this method yielded higher venous signal intensity (and tSNR) and less CSF contamination. The obtained Y_v values are comparable to those reported in the literature[63,66] and have good agreement with the global Y_v measured individually (Table 1).

Higher SNR of local venous blood signal would reduce the error of multi-echo fitting for $T_{2,v}$. Based on the theoretical estimation, the FT-VS–based preparation can intrinsically improve the magnetization of venous blood by 56% over VSS-based approach (0.42 vs. 0.27) (Figure 1), largely driven by employing FT-VSI plus immediate NSI for arterial nulling instead of using VSS followed by NSI after a delay. As explained in the original QUIXOTIC paper,[21] the labeled venous volume depends on both the venous outflow time TO between the 2 VS pulse trains and the employed V_{cut} (the trailing edge). Our experimental results showed 157% and 109% improvement of tSNR of the isolated venous blood signal by the FT-VS preparations with both the higher and lower V_{cut} (0.5 cm/s, 1.4 cm/s) over the VSS-based method (1.0 cm/s). The in vivo tSNR advantage could be in part due to the 45% longer outflow time for the labeled venous bolus, with TO = 1050 ms between the FT-VSI and FT-VSS pulse trains and 725 ms between the first and second VSS pulse trains. Note that to null the arterial blood at 3 T, the TO following the FT-VSI /

TABLE 1 Whole-slice averaged signal intensity, tSNR of the difference image at the second echo, the whole-slice averaged $T_{2,v}$ measured by the FT-VS (V_{cut} = 0.5 and 1.4 cm/s) and VSS (V_{cut} = 1.0 cm/s) experiments, the fitting errors $T_{2,v,error}$, and the correspondingly converted Y_v compared with the global Y_v measured at IJV.

Subject	FT-VS (0.5 cm/s) Signal[a]	tSNR	$T_{2,v}$ (ms)	$T_{2,v,error}$ (ms)	Y_v	FT-VS (1.4 cm/s) Signal[a]	tSNR	$T_{2,v}$ (ms)	$T_{2,v,error}$ (ms)	Y_v	VSS (1.0 cm/s) Signal[a]	tSNR	$T_{2,v}$ (ms)	$T_{2,v,error}$ (ms)	Y_v	Global Y_v
1	1	5.2 ±2.1	56 ±11	5.7 ±4.1	0.60 ±0.06						0.42	2.7 ±1.4	54 ±12	6.7 ±3.4	0.59 ±0.07	0.63
2	1	7.2 ±2.9	63 ±11	4.8 ±2.9	0.60 ±0.05						0.43	3.4 ±1.7	58 ±12	5.7 ±3.6	0.57 ±0.06	0.56
3	1	4.9 ±2.0	59 ±12	4.8 ±2.8	0.62 ±0.07	0.56	3.6 ±1.4	61 ±15	6.2 ±4.0	0.62 ±0.08	0.40	1.6 ±0.9	51 ±12	5.4 ±2.5	0.57 ±0.08	0.63
4	1	6.0 ±2.6	60 ±11	5.3 ±3.4	0.63 ±0.05	0.67	6.1 ±2.5	59 ±14	6.1 ±4.2	0.62 ±0.09	0.36	2.2 ±1.0	59 ±15	6.0 ±3.6	0.62 ±0.09	0.62
5	1	6.6 ±3.3	56 ±11	5.0 ±3.5	0.58 ±0.06	0.83	5.4 ±2.3	56 ±14	5.3 ±3.4	0.56 ±0.09	0.45	1.8 ±1.0	54 ±13	7.2 ±4.7	0.55 ±0.09	0.60
6	1	5.6 ±1.8	59 ±10	6.1 ±4.5	0.62 ±0.05	0.71	4.0 ±1.6	59 ±16	5.3 ±4.8	0.60 ±0.11	0.48	2.1 ±1.2	54 ±14	7.2 ±4.4	0.59 ±0.09	0.57
Mean ±Std	1	5.9 ±0.9	59 ±3	5.3 ±0.5	0.61 ±0.02	0.69 ±0.11	4.8 ±1.2	59 ±2	5.7 ±0.5	0.60 ±0.03	0.42 ±0.04	2.3 ±0.7	55 ±3	6.4 ±0.8	0.58 ±0.02	0.60 ±0.03

[a]The averaged signal intensity of the CSF-corrected difference images at the second echo measured at different experiments normalized by those measured by the FT-VS protocol using V_{cut} = 0.5 cm/s for each volunteer.

FT-VS, Fourier-transform–based velocity-selective; IJV, internal jugular vein; tSNR, temporal SNR; V_{cut} cutoff velocity; VSS, velocity-selective saturation; Y_v, venous oxygenation fraction.

NSI pulses is fixed to be 1050 ms, during which the leading edge of the venous bolus should be still within or close to the voxels of the capillary source, and the measured $T_{2,v}$ values reflect the local venous oxygenation in order to ensure the spatial specificity of the Y_v maps. This condition is supported by the close resemblance between the DIR GM images and the venous blood signal obtained at the second echo in this study (Figures 2, 3) or the vCBV maps derived from the same preparation modules in a prior study.[53] Meanwhile, FT-VS experiments using V_{cut} of 0.5 cm/s had 23% higher venous blood signal (5.9 vs. 4.8) (Table 1) than using V_{cut} of 1.4 cm/s, indicating that lower V_{cut} could increase the venous blood signal being detected. As discussed before,[21] the chosen V_{cut} determines the trailing edge of the venous bolus and ideally should be just above capillary blood velocities (close to 0.1 cm/s[36]) to achieve the maximum available venous signal. However, utilizing a smaller V_{cut} value on clinical scanners is limited by the gradient maximal strength and slew rate as well as potential artifacts caused by eddy current or diffusion mismatch between label and control scans.

CSF contamination is another factor that affects the accuracy of T_2 measurement. To correct CSF contamination, Stout et al.[22] applied a fixed magnetization fraction of CSF in all GM voxels (0.112) obtained from a separate calibration experiment. Instead, our protocol observed about ∼20%–40% CSF fractions contained in the difference images through direct estimation (Supporting Information Table S1). The measured average CSF T_2 for all our volunteers was 1.2 ± 0.2 s, which is comparable to previously measured T_2 values of CSF in brain tissue.[22,54,60] Therefore, instead of employing an extra scan to map CSF T_2, it would be faster and simpler to just use 1.2 s as a fixed CSF T_2 value for all voxels.

To accurately measure Y_v, conversion of venous blood T_2 value to Y_v is also very important. The $T_{2,v}$ value depends highly on the interval between the refocusing pulses (τ). Currently, however, blood T_2-Y_v calibration curves[66,67] are available for only a limited set of τ values. This induces the inconvenience of choosing the interval between refocusing pulses, especially for our multi-echo acquisition design in which the interval of refocusing pulses is limited by other acquisition parameters. Recently, a blood T_2-Y_v model[64] has been proposed that can calculate blood T_2 based on B_0, τ, and Hct with good agreement with previous experimental results. A website[57] is also available to conveniently convert blood T_2 to Y_v. Note that Hct measured from blood T_1 values is an efficient noninvasive approach that not only facilitates T_2-Y_v calibration but also assists evaluation of the between-subject variations for perfusion and functional MRI studies.[65]

Despite of achieving higher SNR than VSS-based method, to ensure acceptable levels of accuracy and precision for the Y_v estimation per voxel, the current FT-VS–based T2-oximetry method only acquired a single slice Y_v map with a low spatial resolution (voxel size of $7.9 \times 7.9 \times 10.0$ mm^3) over 5 min. Although the current spatial resolution is comparable to the range in [^{15}O]-gas PET studies,[68] further technical development is still warranted to extend its implementation from 2D single-slice imaging to 3D whole-brain coverage using segmented acquisitions to ensure wider utility of this method for clinical use. Denoising with deep-learning approach[69,70] can also be employed for obtaining higher spatial resolution.

5 | CONCLUSION

Employing advanced velocity-selective pulse trains, an improved venous oxygenation mapping technique is proposed with minimal sensitivity to arterial transit delay, high venous signal, and mitigation of CSF contamination, which are important to improve the accuracy and precision of $T_{2,v}$ measurements. The estimated Y_v values are similar between GM and WM and comparable to the values measured globally.

CONFLICT OF INTEREST

Dr. van Zijl is a paid lecturer for Philips Healthcare, has research support from Philips, and has technology licensed to Philips. This has been approved by the Committee on Conflict of Interest of Johns Hopkins University.

ORCID
Feng Xu https://orcid.org/0000-0001-7958-3787
Dan Zhu https://orcid.org/0000-0002-0940-1519
Qin Qin https://orcid.org/0000-0002-6432-2944

REFERENCE

1. An H, Lin W. Impact of intravascular signal on quantitative measures of cerebral oxygen extraction and blood volume under normo- and hypercapnic conditions using an asymmetric spin echo approach. *Magn Reson Med*. 2003;50:708-716.
2. Yin Y, Zhang Y, Gao J-H. Dynamic measurement of oxygen extraction fraction using a multiecho asymmetric spin echo (MASE) pulse sequence. *Magn Reson Med*. 2018;80:1118-1124.
3. Davis TL, Kwong KK, Weisskoff RM, Rosen BR. Calibrated functional MRI: mapping the dynamics of oxidative metabolism. *Proc Natl Acad Sci U S A*. 1998;95:1834-1839.
4. Hoge RD. Calibrated fMRI. *Neuroimage*. 2012;62:930-937.
5. Gauthier CJ, Hoge RD. Magnetic resonance imaging of resting OEF and CMRO$_2$ using a generalized calibration model for hypercapnia and hyperoxia. *Neuroimage*. 2012;60:1212-1225.

6. Bulte DP, Kelly M, Germuska M, et al. Quantitative measurement of cerebral physiology using respiratory-calibrated MRI. *Neuroimage*. 2012;60:582-591.

7. Blockley NP, Griffeth VEM, Simon AB, Buxton RB. A review of calibrated blood oxygenation level-dependent (BOLD) methods for the measurement of task-induced changes in brain oxygen metabolism. *NMR Biomed*. 2013;26:987-1003.

8. He X, Yablonskiy DA. Quantitative BOLD: mapping of human cerebral deoxygenated blood volume and oxygen extraction fraction: default state. *Magn Reson Med*. 2007;57:115-126.

9. Christen T, Lemasson B, Pannetier N, et al. Evaluation of a quantitative blood oxygenation level-dependent (qBOLD) approach to map local blood oxygen saturation. *NMR Biomed*. 2011;24:393-403.

10. An H, Lin W. Cerebral oxygen extraction fraction and cerebral venous blood volume measurements using MRI: effects of magnetic field variation. *Magn Reson Med*. 2002;47:958-966.

11. Yablonskiy DA, Sukstanskii AL, He X. Blood oxygenation level-dependent (BOLD)-based techniques for the quantification of brain hemodynamic and metabolic properties - theoretical models and experimental approaches. *NMR Biomed*. 2013;26:963-986.

12. Kudo K, Liu T, Murakami T, et al. Oxygen extraction fraction measurement using quantitative susceptibility mapping: comparison with positron emission tomography. *J Cereb Blood Flow Metab*. 2016;36:1424-1433.

13. Fan AP, Benner T, Bolar DS, Rosen BR, Adalsteinsson E. Phase-based regional oxygen metabolism (PROM) using MRI. *Magn Reson Med*. 2012;67:669-678.

14. Fan AP, Bilgic B, Gagnon L, et al. Quantitative oxygenation venography from MRI phase. *Magn Reson Med*. 2014;72:149-159.

15. Zhang J, Liu T, Gupta A, Spincemaille P, Nguyen TD, Wang Y. Quantitative mapping of cerebral metabolic rate of oxygen (CMRO2) using quantitative susceptibility mapping (QSM). *Magn Reson Med*. 2015;74:945-952.

16. Zhang J, Cho J, Zhou D, et al. Quantitative susceptibility mapping-based cerebral metabolic rate of oxygen mapping with minimum local variance. *Magn Reson Med*. 2018;79:172-179.

17. Zhang J, Zhou D, Nguyen TD, Spincemaille P, Gupta A, Wang Y. Cerebral metabolic rate of oxygen (CMRO2) mapping with hyperventilation challenge using quantitative susceptibility mapping (QSM). *Magn Reson Med*. 2017;77:1762-1773.

18. Cho J, Kee Y, Spincemaille P, et al. Cerebral metabolic rate of oxygen (CMRO2) mapping by combining quantitative susceptibility mapping (QSM) and quantitative blood oxygenation level-dependent imaging (qBOLD). *Magn Reson Med*. 2018;80:1595-1604.

19. Cho J, Zhang S, Kee Y, et al. Cluster analysis of time evolution (CAT) for quantitative susceptibility mapping (QSM) and quantitative blood oxygen level-dependent magnitude (qBOLD)-based oxygen extraction fraction (OEF) and cerebral metabolic rate of oxygen (CMRO2) mapping. *Magn Reson Med*. 2020;83:844-857.

20. Cho J, Lee J, An H, Goyal MS, Su Y, Wang Y. Cerebral oxygen extraction fraction (OEF): comparison of challenge-free gradient echo QSM+qBOLD (QQ) with 15O PET in healthy adults. *J Cereb Blood Flow Metab*. 2021;41(4):1658-1668.

21. Bolar DS, Rosen BR, Sorensen AG, Adalsteinsson E. QUantitative imaging of eXtraction of oxygen and TIssue consumption (QUIXOTIC) using venular-targeted velocity-selective spin labeling. *Magn Reson Med*. 2011;66:1550-1562.

22. Stout JN, Adalsteinsson E, Rosen BR, Bolar DS. Functional oxygen extraction fraction (OEF) imaging with turbo gradient spin echo QUIXOTIC (turbo QUIXOTIC). *Magn Reson Med*. 2018;79:2713-2723.

23. Guo J, Wong EC. Venous oxygenation mapping using velocity-selective excitation and arterial nulling. *Magn Reson Med*. 2012;68:1458-1471.

24. Liu EY, Guo J, Simon AB, Haist F, Dubowitz DJ, Buxton RB. The potential for gas-free measurements of absolute oxygen metabolism during both baseline and activation states in the human brain. *Neuroimage*. 2020;207:116342.

25. Oja JM, Gillen JS, Kauppinen RA, Kraut M, van Zijl PC. Determination of oxygen extraction ratios by magnetic resonance imaging. *J Cereb Blood Flow Metab*. 1999;19:1289-1295.

26. Lu H, Ge Y. Quantitative evaluation of oxygenation in venous vessels using T2-relaxation-under-spin-tagging MRI. *Magn Reson Med*. 2008;60:357-363.

27. Wright GA, Hu BS, Macovski A. Estimating oxygen saturation of blood in vivo with MR imaging at 1.5 T. *J Magn Reson Imaging*. 1991;1:275-283.

28. Sharan M, Jones MD, Koehler RC, Traystman RJ, Popel AS. A compartmental model for oxygen transport in brain microcirculation. *Ann Biomed Eng*. 1989;17:13-38.

29. Van Zijl PCM, Eleff SM, Ulatowski JA, et al. Quantitative assessment of blood flow, blood volume and blood oxygenation effects in functional magnetic resonance imaging. *Nat Med*. 1998;4:159-167.

30. Piechnik SK, Chiarelli PA, Jezzard P. Modelling vascular reactivity to investigate the basis of the relationship between cerebral blood volume and flow under CO2 manipulation. *Neuroimage*. 2008;39:107-118.

31. Priest AN, Graves MJ, Lomas DJ. Non-contrast-enhanced vascular magnetic resonance imaging using flow-dependent preparation with subtraction. *Magn Reson Med*. 2012;67:628-637.

32. Fan Z, Hodnett PA, Davarpanah AH, et al. Noncontrast magnetic resonance angiography of the hand. *Invest Radiol*. 2011;46:515-523.

33. Fan Z, Sheehan J, Bi X, Liu X, Carr J, Li D. 3D noncontrast MR angiography of the distal lower extremities using flow-sensitive dephasing (FSD)-prepared balanced SSFP. *Magn Reson Med*. 2009;62:1523-1532.

34. Duhamel G, De Bazelaire C, Alsop DC. Evaluation of systematic quantification errors in velocity-selective arterial spin labeling of the brain. *Magn Reson Med*. 2003;50:145-153.

35. Wong EC, Cronin M, Wu W-C, Inglis B, Frank LR, Liu TT. Velocity-selective arterial spin labeling. *Magn Reson Med*. 2006;55:1334-1341.

36. Liu D, Xu F, Lin DD, van Zijl PCM, Qin Q. Quantitative measurement of cerebral blood volume using velocity-selective pulse trains. *Magn Reson Med*. 2017;77:92-101.

37. Lee H, Wehrli FW. Venous cerebral blood volume mapping in the whole brain using venous-spin-labeled 3D turbo spin echo. *Magn Reson Med*. 1991;2020:2003.

38. Shin T, Hu BS, Nishimura DG. Off-resonance-robust velocity-selective magnetization preparation for non-contrast-enhanced peripheral MR angiography. *Magn Reson Med*. 2013;70:1229-1240.

39. Shin T, Worters PW, Hu BS, Nishimura DG. Non-contrast-enhanced renal and abdominal MR angiography using velocity-selective inversion preparation. *Magn Reson Med*. 2013;69:1268-1275.

40. Qin Q, Shin T, Schär M, Guo H, Chen H, Qiao Y. Velocity-selective magnetization-prepared non-contrast-enhanced cerebral MR angiography at 3 Tesla: improved immunity to B0/B1 inhomogeneity. *Magn Reson Med*. 2016;75: 1232-1241.

41. Shin T, Qin Q, Park JY, Crawford RS, Rajagopalan S. Identification and reduction of image artifacts in non–contrast-enhanced velocity-selective peripheral angiography at 3T. *Magn Reson Med*. 2016;76:466-477.

42. Li W, Xu F, Schär M, et al. Whole-brain arteriography and venography: using improved velocity-selective saturation pulse trains. *Magn Reson Med*. 2018;79:2014 2023.

43. Shin T, Qin Q. Characterization and suppression of stripe artifact in velocity-selective magnetization-prepared unenhanced MR angiography. *Magn Reson Med*. 2018;80:1997-2005.

44. Zhu D, Li W, Liu D, et al. Non-contrast-enhanced abdominal MRA at 3 T using velocity-selective pulse trains. *Magn Reson Med*. 2020;84:1173-1183.

45. Qin Q, van Zijl PCM. Velocity-selective-inversion prepared arterial spin labeling. *Magn Reson Med*. 2016;76:1136-1148.

46. Liu D, Xu F, Li W, van Zijl PCM, Lin DD, Qin Q. Improved velocity-selective-inversion arterial spin labeling for cerebral blood flow mapping with 3D acquisition. *Magn Reson Med*. 2020;84:2512-2522.

47. Hernandez-Garcia L, Nielsen JF, Noll DC. Improved sensitivity and temporal resolution in perfusion FMRI using velocity selective inversion ASL. *Magn Reson Med*. 2019;81: 1004-1015.

48. Landes V, Javed A, Jao T, Qin Q, Nayak K. Improved velocity-selective labeling pulses for myocardial ASL. *Magn Reson Med*. 2020;84:1909-1918.

49. Franklin SL, Bones IK, Harteveld AA, et al. Multi-organ comparison of flow-based arterial spin labeling techniques: spatially non-selective labeling for cerebral and renal perfusion imaging. *Magn Reson Med*. 2021;85:2580-2594.

50. Guo J, Das S, Hernandez-Garcia L. Comparison of velocity-selective arterial spin labeling schemes. *Magn Reson Med*. 2021;85:2027-2039.

51. Liu D, Li W, Xu F, Zhu D, Shin T, Qin Q. Ensuring both velocity and spatial responses robust to B0/B1+ field inhomogeneities for velocity-selective arterial spin labeling through dynamic phase-cycling. *Magn Reson Med*. 2021;85:2723-2734.

52. Qin Q, Qu Y, Li W, et al. Cerebral blood volume mapping using Fourier-transform–based velocity-selective saturation pulse trains. *Magn Reson Med*. 2019;81:3544-3554.

53. Li W, van Zijl PC, Qin Q. Three-dimensional whole-brain mapping of cerebral blood volume and venous cerebral blood volume using fourier-transform based velocity-selective pulse trains. *Magn Reson Med*. 2021;86:1420-1433.

54. Guo J, Wong EC. Removal of CSF contamination in VSASL and QUIXOTIC using a long TE CSF scan. In Proceedings of the 19th Annual Meeting of ISMRM, Montréal, Québec, Canada, 2011. p. 2116.

55. Ogg RJ, Kingsley PB, Taylor JS. WET, a T1- and B1-insensitive water-suppression method for in vivo localized 1H NMR spectroscopy. *J Magn Reson Ser B*. 1994;104:1-10.

56. Li W, Grgac K, Huang A, Yadav N, Qin Q, Van Zijl PCM. Quantitative theory for the longitudinal relaxation time of blood water. *Magn Reson Med*. 2016;76:270-281.

57. Li W, van Zijl P. Blood T2, T1 calculator. Available at: http://godzilla.kennedykrieger.org/cgi-bin/bloodT2T1_cal.pl. Published November 1 2021.

58. Levitt M, Freeman R, Frenkiel T. Broadband heteronuclear decoupling. *J Magn Reson*. 1983;51:56-66.

59. Hennig J. Echoes—how to generate, recognize, use or avoid them in MR-imaging sequences. Part II: echoes in imaging sequences. *Concepts Magn Reson*. 1991;3:179-192.

60. Qin Q. A simple approach for three-dimensional mapping of baseline cerebrospinal fluid volume fraction. *Magn Reson Med*. 2011;65:385-391.

61. Redpath TW, Smith FW. Technical note: use of a double inversion recovery pulse sequence to image selectively grey or white brain matter. *Br J Radiol*. 1994;67:1258-1263.

62. Qin Q, Strouse JJ, van Zijl PCM. Fast measurement of blood T1 in the human jugular vein at 3 tesla. *Magn Reson Med*. 2011;65:1297-1304.

63. Qin Q, Grgac K, van Zijl PCM. Determination of whole-brain oxygen extraction fractions by fast measurement of blood T(2) in the jugular vein. *Magn Reson Med*. 2011;65:471-479.

64. Li W, van Zijl PCM. Quantitative theory for the transverse relaxation time of blood water. *NMR Biomed*. 2020;33:4207.

65. Xu F, Li W, Liu P, et al. Accounting for the role of hematocrit in between-subject variations of MRI-derived baseline cerebral hemodynamic parameters and functional BOLD responses. *Hum Brain Mapp*. 2018;39:353.

66. Lu H, Xu F, Grgac K, Liu P, Qin Q, van Zijl PCM. Calibration and validation of TRUST MRI for the estimation of cerebral blood oxygenation. *Magn Reson Med*. 2012;67:42-49.

67. Bush A, Borzage M, Detterich J, et al. Empirical model of human blood transverse relaxation at 3 T improves MRI T2 oximetry. *Magn Reson Med*. 2017;77:2364-2371.

68. Fan AP, An HY, Moradi F, et al. Quantification of brain oxygen extraction and metabolism with [O-15]-gas PET: a technical review in the era of PET/MRI. *Neuroimage*. 2020; 220:117136.

69. Xie DF, Li YR, Yang HL, et al. Denoising arterial spin labeling perfusion MRI with deep machine learning. *Magn Reson Imaging*. 2020;68:95-105.

70. Gong EH, Guo J, Liu J, Fan A, Pauly J, Zaharchuk G. Deep learning and multi-contrast based denoising for low-SNR arterial spin labeling (ASL) MRI. In Proceedings of SPIE, Medical Imaging 2020: Houston, Texas, 2020. p. 11313.

SUPPORTING INFORMATION

Additional supporting information may be found in the online version of the article at the publisher's website.

Figure S1: (a) The diagrams of the 2D CSF T2 mapping method, including a slab-selective pre-saturation with a post-saturation delay (9000 ms), a T2 preparation (600 ms) to suppress other tissues with short T2s, fat-suppression, and a multi-echo readout with 16 pairs of hyperbolic tangent (HT) refocusing pulses (total of 32 echoes, echo spacing = 15 ms).

Figure S2: Calculation (a) and demonstration (b) of a multiplication coefficient to correct the T2 overestimation due to the 4 ms pulse length of HT refocusing pulses during the 15 ms refocusing interval.

Table S1: The whole-slice averaged remaining CSF fraction in the difference images at the 2ndecho by FT-VS (Vcut = 0.5 and 1.4 cm/s) and VSS (Vcut = 1.0 cm/s) experiments.